Chemical Engineering Journal 220 (2013) 431–440

Contents lists available at SciVerse ScienceDirect

Chemical Engineering Journal

journal homepage: www.elsevier.com/locate/cej

Air–water mass transfer of sparingly soluble odorous compounds in granular biofilter media

Rune R. Andreasen [a,*], Dezhao Liu [b], Sebastian Ravn [a], Anders Feilberg [b], Tjalfe G. Poulsen [a]

[a] Department of Chemistry, Biotechnology and Environmental Engineering, Aalborg University, Sohngaardsholmsvej 57, DK-9000, Denmark
[b] Department of Engineering, Aarhus University, Blichers Allé 20, DK-8830, Denmark

HIGHLIGHTS

- Air–water mass transfer was measured for individual hydrophobic odorous compounds without using chemical reactions.
- Mass transfer increased with increasing gas phase velocity, media specific surface area and compound solubility.
- Mass transfer was satisfactorily modeled across three gas velocities, six compounds and seven medium particle size distributions.

ARTICLE INFO

Article history:
Received 5 September 2012
Received in revised form 12 December 2012
Accepted 30 December 2012
Available online 23 January 2013

Keywords:
Mass transfer
Biological air filter
PTR-MS
Volatile sulfur compounds
Particle size distribution
Filter air velocity

ABSTRACT

Mass transfer from air to the liquid phase is a key parameter controlling the efficiency of air cleaning biofilters. Especially the removal of sparingly soluble organic compounds such as volatile odorous sulfur compounds is mass transfer limited. When determining mass transfer rates of sparingly soluble organic compounds the approach have been to either conduct measurements using highly soluble compounds or sparingly soluble compounds with chemical removal of the compounds in the water phase to maintain maximum mass transfer. These data may, therefore, not represent the correct mass transfer rates for sparingly soluble compounds. As a consequence existing mass transfer models may not be accurate for these compounds. In addition most studies of mass transfer in granular media are based on materials consisting of uniform particles. This study investigates the impact of particle size (considering materials with multiple particle sizes), gas velocity and contaminant chemical properties on the overall volumetric mass transfer coefficient based on direct measurements (without the use of chemical reactions) of volatile, sparingly soluble, odorous organic compounds in granular media. Mass transfer was found closely related to particle size, compound solubility, particle size range, specific surface area and gas velocity. Predictive models linking mass transfer, gas velocity, contaminant solubility, media specific surface area, particle size and medium CO_2 mass transfer were developed.

1. Introduction

During recent decades global pork production has increased rapidly with the annual production exceeding 100 million tons in 2005 (a 50% increase over the previous 15 years [2]). Also pig farms have increased in size producing increased emissions of air-borne odorous compounds, a source of nuisance to people living in the vicinity, thus, increasing the pressure for reducing odor emissions [3]. Odor emissions are primarily associated with the large quantities of ventilation air from the animal facilities [4]. At present biofiltration seems to be one of the most cost effective technologies for odor removal from the exhaust air [4,5]. Biofilter efficiency is closely connected to the biofilter reactors volumetric elimination capacity (mol s^{-1} m^{-3}). The volumetric elimination capacity is generally controlled by either the microbial degradation rate or the rate of mass transfer across the gas–liquid interface [6]. In air fed biofilters the overall volumetric mass transfer across the air–water interface ($K_G a_e$ (mol s^{-1} m^{-2} (mol m^{-3})$^{-1}$ (m^2 m^{-3})) or simply (s^{-1})) is proportional to the contaminant solubility in the water phase [6]. The efficiency of biofilters for removal of sparingly soluble odorous compounds such as H_2S or methane thiol's is therefore likely to be limited by the air–water interface mass transfer [7]. $K_G a_e$ is closely linked to medium specific surface area, a (m^2 m^{-3}) [8] and can easily be increased by increasing a for instance by decreasing filter material particle size. However, decreasing the particle size will also increase the air pressure drop across the biofilter [1,9] thereby increasing filter energy consumption and operation costs [5,10,11]. Optimization of biofilter cost-efficiency is, thus, a trade-off, between contaminant removal efficiency and operation

* Corresponding author. Tel.: +45 9640 8493; fax: +45 9635 0558.
E-mail address: rra@bio.aau.dk (R.R. Andreasen).

1385-8947/$ - see front matter © 2013 Elsevier B.V. All rights reserved.
http://dx.doi.org/10.1016/j.cej.2012.12.087

Nomenclature

A	filter cross sectional area (m^2)
a	filter medium specific surface area ($m^2\ m^{-3}$)
C	contaminant concentration ($mol\ m^{-3}$)
D	contaminant diffusivity in the respective phases ($m^2\ s^{-1}$)
d	particle diameter
d_{eq}	equivalent particle diameter, as defined by Ref. [1] (m)
d_m	mean particle diameter (m)
D_p	dispersion–diffusion coefficient ($m^2\ s^{-1}$)
d_p	characteristic packing length (m)
Fr	Froude number
g	gravitational acceleration ($9.81\ m\ s^{-2}$)
H	Henrys constant ($mol_{gas}\ m^{-3}_{gas}$) ($mol_{liquid}\ m^{-3}_{liquid}$)$^{-1}$ or (–).
K_G, k_l, k_g	overall, -liquid-side and -gas-side mass transfer coefficients ($mol\ s^{-1}\ m^{-2}$ ($mol\ m^{-3}$)$^{-1}$ ($m^2\ m^{-3}$)) or simply (s^{-1})
K_Ga_e, k_la_e, k_ga_e	volume specific- overall, -liquid-side and -gas-side mass transfer coefficients ($mol\ s^{-1}\ m^{-2}$ ($mol\ m^{-3}$)$^{-1}$) or simply ($m\ s^{-1}$)
M_{tot}	total particle mass (g)
Q	flow rate ($m^3\ s^{-1}$)
R	particle size range (m)
Re	Reynolds number (–)
u	pore air velocity ($m\ s^{-1}$)
V	superficial air or water velocity ($m\ s^{-1}$)
We	Weber number (–)
z	filter depth (m)
k	empirical determined mass transfer coefficient (K_Ga_e, k_la_e or k_ga_e)
P	parameter for empirical fit

Greek letters

α	empirical constant (–)
β	empirical constant (–)
ε_{ex}	external air-filled porosity ($m^3\ m^{-3}$)
θ	volumetric water content ($m^3\ m^{-3}$)
μ	viscosity ($N\ s\ m^{-1}$)
ρ	density ($kg\ m^{-3}$)
σ_C	critical surface tension of the packing material ($N\ m^{-1}$)
σ_l	surface tension of the liquid ($N\ m^{-1}$)

Subscripts

b	bulk
e	effective
l	liquid phase
g	gas phase
p	particle

costs. To make this trade-off, knowledge of K_Ga_e is essential. The mass transfer coefficient depends on the fluid flow characteristics in both the air and water phases and is therefore closely linked to the Reynolds number (Re, (–)) and thereby the fluid velocity (V, ($m\ s^{-1}$)) in both phases [8]. While the gas flow rate, Q_g ($m^3\ s^{-1}$), for animal production facilities can vary with up to a factor of 10, partly controlled by weather conditions [4], the biofilter water flow (if any) as well as media characteristics such as a are often relatively stable. It is therefore most likely that the main variation in K_Ga_e of an operating biofilter will be caused by variations in Q_g. Knowledge of the K_Ga_e–Q_g relationship can therefore be highly valuable for designing of future biofilters and biofilter media. Values of K_Ga_e for a given medium, contaminant and filter operating conditions can be either measured or predicted using an appropriate model. Since many odorous compounds are only sparingly soluble in water, direct measurements (as without chemical removal of the compounds in the water phase) of K_Ga_e for these compounds is difficult to do accurately. In such cases a model for predicting K_Ga_e is very useful. Onda et al. [8] proposed a model for predicting K_Ga_e as a function of medium, contaminant, and filter operational characteristics. Kim and Deshusses [12] however, found the Onda et al. [8] equation to over-predict K_Ga_e of several suitable biofilter materials (lava rock, cylindrical pall rings, polyurethane foam cubes, porous ceramic beads/rasching rings and compost/woodchips mixtures) by a factor 3–20. Kim and Deshusses [12] therefore proposed a simplified empirical expression, based on a power function with two empirical constants, unique for each packing material. Based on various biofilter packing media (lava rock, Dixon rings, polyurethane foam cubes and clay pellets), Dorado et al.[13] evaluated several existing expressions for predicting K_Ga_e, including Onda et al. [8] and Kim and Deshusses [12], and found all included correlations to have unsatisfactory K_Ga_e prediction accuracy. Dorado et al. [13] therefore recommended future K_Ga_e prediction to be based on experimental data fitted to simple mathematical expressions.

At present knowledge of the relationship between biofilter K_Ga_e, gas phase velocity V_g ($m\ s^{-1}$), and media particle size distribution is limited, especially for sparingly soluble odorous compounds which to the author's knowledge have not yet been studied through direct measurements.

With the recommendation to use simple mathematical correlations for predicting K_Ga_e [13], the aim of this study is to develop a simple empirical model concept for predicting K_Ga_e as a function of V_g, contaminant chemical properties, and media characteristics (particle size distribution, specific surface area, etc.) using the model by Kim and Deshusses [12] as a starting point. The empirical model constants are to be valid across media with different particle size distributions provided they belong to the same type of packing material. This model will allow easier K_Ga_e prediction across numerous particle size distributions compared to the Kim and Deshusses [12] correlation which requires a new set of empirical constants for each particle size distribution considered. The model will be developed based on breakthrough measurements of sparingly soluble odorous compounds as at present only a few K_Ga_e studies [13] have focused on direct measurements of such sparingly soluble compounds and to the authors knowledge none have been focusing on sparingly soluble odorous compounds, despite their obvious relevance. Such a model will be a valuable tool when designing biofilter media and constructing biofilters with the aim of selecting the optimal filter media and dimensions. The model will be developed based on measurements of the mass transfer behavior of selected sparingly soluble compounds including a range of common odorous compounds found in exhaust air from pig production facilities, using granular biofilter media with different particle sizes for a range of different air flow rates. Finally will K_Ga_e be linked to an easier determinable mass transfer parameter, in order to enable easy K_Ga_e estimations. The model for prediction of K_Ga_e will be based on direct measurements of the mass transfer behavior of sparingly soluble compounds. As the removal of sparingly soluble compounds are facilitated by low water content (results in low water film thickness) the measurements will be based on extremely low irrigation velocities to simulate practical conditions [14]. A commercially available medium: Light Expanded Clay Aggregates (Leca®) consisting of porous rounded aggregates available in sizes from 2 to 18 mm with similar shape was selected as biofilter medium in this study. The advantage of this material is

that it is available with a well-defined mean particle size, it is not subject to degradation over time and it has a relatively large specific surface area. It has been successfully used in industrial biofilters at a meat rendering plant [15] and is currently being applied for air cleaning at pig production facilities [16,17]. As the focus of this study is the relationship between the air–water mass transfer rate and the filter material properties, measurements will be carried out under conditions where no biomass is present. It is recognized that the presence of biomass is likely to affect $K_G a_e$ [18–20]. However this is considered beyond the scope of this paper.

2. Theory

The convection–dispersion equation for gas flow through porous homogeneous biofilter media with insignificant adsorption, degradation and stagnant air volumes is [21]:

$$\frac{\partial C_g}{\partial t} = D_p \frac{\partial^2 C_g}{\partial z^2} - u\frac{\partial C_g}{\partial z} \tag{1}$$

where C_g is gas phase concentrations (mol m^{-3}), D_p is the dispersion diffusion coefficient (m^2 s^{-1}), z and t is the space (m) and time (s) variables and u is the pore gas velocity (m s^{-1}) defined as:

$$u = V_g \frac{1}{\varepsilon_{ex}} = \frac{Q_g}{A}\frac{1}{\varepsilon_{ex}} \tag{2}$$

where V_g is the gas velocity, A (m^2) is the cross section area perpendicular to the direction of flow and ε_{ex} is the external porosity (m^3 m^{-3}) assumed equal to air-filled flow conducting porosity.

Biofilters often contains both a gas and a liquid phase. At equilibrium conditions the concentration in these two phases are directly proportional as described by Henry's law:

$$C_l = C_g H^{-1} \tag{3}$$

where C_l is the liquid phase concentration (mol_l m_l^{-3}) and H is the Henry's constant (mol_g m_g^{-3} mol_l^{-1} m_l^3) or simply (–).

In a system (such as bio and biotrickling filters) with contaminant transport between a mobile gas phase and an immobile liquid phase (Eq. (1)) changes to:

$$\frac{\partial C_g}{\partial t} = D_p \frac{\partial^2 C_g}{\partial z^2} - u\frac{\partial C_g}{\partial z} - K_G a_e (C_g - C_l H) \tag{4a}$$

where $K_G a_e$ is the overall volumetric mass transfer coefficient (mol s^{-1} m^{-2} (mol m^{-3})$^{-1}$ (m^2 m^{-3})) or simply (s^{-1}) and C_l is described by:

$$\frac{\partial C_l}{\partial t} = K_G a_e (C_g - C_l H)\frac{\varepsilon_{ex}}{\theta_a} \tag{4b}$$

where θ_a is filter active water content (m^3 m^{-3}) contributing to the dissolution of contaminants.

Under steady state conditions $\left(\frac{\partial C_g}{\partial t} = 0\right)$ with $C_l = 0$, and neglecting gas phase dispersion, C_g as a function of residence time, follows a first order expression. For this reason determination of mass transfer coefficients are often based on measurements of gas absorption where the dissolved gas is removed by a fast chemical reaction to achieve $C_l \approx 0$. In such cases $K_G a_e$ can be determined as [22]:

$$K_G a_e = \frac{u}{z}\ln\left(\frac{C_{g,inlet}}{C_{g,outlet}}\right) \tag{5}$$

According to the generally applied two film theory [23] $K_G a_e$ consist of a liquid side mass transfer coefficient ($k_l a_e$, (s^{-1})) and a gas side mass transfer coefficient ($k_g a_e$, (s^{-1})) as:

$$\frac{1}{K_G a_e} = \frac{1}{k_g a_e} + \frac{H}{k_l a_e} \tag{6}$$

As the liquid side resistance (H $k_l a_e^{-1}$) is directly proportional to H, H has a large impact on whether the mass transfer for a given contaminant is limited by the gas side resistance ($k_g a_e^{-1}$), liquid side resistance or both. Transfer of highly volatile compounds is generally limited by $k_l a_e$, while $k_g a_e$ limits exchange of highly soluble compounds [24]. Eq. (6) further implies that $K_G a_e$ and H are inversely related if $K_G a_e$ is limited by the liquid side transfer (H $k_l a_e^{-1} \gg k_g a_e^{-1}$) while $K_G a_e$ is independent of H if $k_g a_e$ is limiting (H $k_l a_e^{-1} \ll k_g a_e^{-1}$).

$K_G a_e$ is the product of medium specific overall mass transfer coefficient K_G (mol s^{-1} m^{-2} (mol m^{-3})$^{-1}$) and the effective air–water interfacial area (a_e) (m^2 m^{-3}). As a_e is rather difficult to measure accurately in coarse granular media, and as $K_G a_e$ rather than K_G is of interest for biofilter designers this paper will focus on $K_G a_e$ rather than K_G and a_e separately. This is also the case for $k_g a_e$ and $k_l a_e$. Several expressions for predicting $K_G a_e$ have been suggested [25]. The first and still widely used expression was suggested by Onda et al. [8] and has been found to fit experimental data well in several studies [24,26,27]. The Onda et al. [8] expression is given as:

$$k_g a_e = a_e \alpha \left(\frac{V_g \rho_g}{a \mu_g}\right)^{0.7}\left(\frac{\mu_g}{\rho_g D_g}\right)^{1/3}(a d_p)^{-2} a D_g \tag{7}$$

$$k_l a_e = a_e 0.0051\left(\frac{V_l \rho_l}{a_e \mu_l}\right)^{2/3}\left(\frac{\mu_l}{\rho_l D_l}\right)^{-1/2}(a d_p)^{0.4}\left(\frac{\rho_l}{\mu_l g}\right)^{-1/3} \tag{8}$$

where Onda et al. [22] assumed a_e equal to the wet specific surface area which is given as:

$$a_e = a\left[1 - \mathrm{Exp}\left(-1.45\left(\frac{\sigma_C}{\sigma_l}\right)^{0.75}\mathrm{Re}_l^{0.1}\mathrm{Fr}_l^{-0.05}\mathrm{We}_l^{0.2}\right)\right] \tag{9}$$

where ρ is the fluid density (kg m^{-3}), μ is fluid viscosity (N s m^{-1}), D is contaminant diffusivity (m^2 s^{-1}), d_p is the characteristic packing length (m), α is an empirical constant = 2 for $d_p < 15$ mm and 5.23 for $d_p > 15$ mm, g is the gravitational constant (9.81 m s^{-2}), σ_l is the surface tension of the liquid (N m^{-1}), σ_C is the critical surface tension of the packing material (N m^{-1}) and Re, Fr, and We is the liquid Reynolds, Froude, and Weber numbers (–), respectively.

Later Bravo and Fair [28] observed that a_e increased with increasing gas velocity and proposed that this was due to water surface rippling and liquid droplet dispersion caused by the increased energy in the gas as:

$$a_e = 0.498 a\left(\frac{\sigma_l^{0.5}}{z^{0.4}}\right)\left(\frac{\mu_l V_l}{\sigma_l}\frac{6 V_g \rho_g}{a \mu_g}\right)^{0.392} \tag{10}$$

where z is the filter thickness (m).

The Onda et al. [8] correlations were extracted from gas/liquid contactors with Re_L and Re_G in the range of 1–1000 and 1–800, respectively. These Re_L values, however, are in general higher than those applied in full-scale, low liquid velocity biotrickling filters (often denoted as biofilters) and studies [12,13,29] where $0.01 < Re_L < 15$ (this study, $0.005 < Re_L < 0.025$). Likewise are the Re_G applied in relevant bio and biotrickling filters and studies [12,13,29] where $0.01 < Re_L < 500$ (this study, $6 < Re_G < 89$), in the lower range of the Re_G applied in Onda et al. [8].

Though Onda et al. [8] found the majority of the measured $k_g a_e$ and $k_l a_e$ data to fall within 20% of the prediction span Kim and Deshusses [12] found the Onda et al. [8] correlation to over predict $k_g a_e$ and $k_l a_e$ by a factor 3–20 when applying it to a set of different materials. To reduce this error a simplified expression for relating $k_g a_e$ with V_g or $k_l a_e$ with V_l using a simple power function was suggested by Kim and Deshusses [12] as:

$$k = \alpha P^{\beta} \quad (11)$$

where k is the mass transfer coefficient of interest ($k_g a_e$ or $k_l a_e$) P is parameter used in the correlation (V_g or V_l) and α and β are empirical constants that depend on the relationship modeled as well as on the filter medium used.

The Onda et al. [8] $k_g a_e$–V_g, relationship (Eq. (7)) corresponds to Eq. (11) with $\beta = 0.7$ for a medium consisting uniform spherical particles ($a = 6(1 - \varepsilon_{ex}) d_p^{-1}$). Using data sets for different media Kim and Deshusses [12] observed β for $k = k_g a_e$ and $P = V_g$ in the range of 0.02–0.75.

3. Materials and methods

3.1. Filter materials used

Mass transfer coefficients in granular biofilter media was investigated using a commercially available material, Leca® (Light Expanded Clay Aggregates), which is used for multiple purposes including insulation and biofiltration [7]. Leca® consists of porous rounded, particles with high internal porosity of which the majority are intra particle (internal) pores which are either very small or not connected with the external air filled pores (ε_{ex}, ($m^3\ m^{-3}$)) and therefore do not conduct air. This material was chosen as it represents a wide range of both artificial and natural (stones, pebbles) granular biofilter materials. Saint-Gobain Weber A/S Randers, Denmark, provided the Leca® used in this study in 8 pre-sorted particle size fractions each with a uniform particle size distribution. These fractions had a particle size range (R, (m)) of 2 mm, and particle diameters (d, (m)) of $2 \leqslant d < 4$ mm, $4 \leqslant d < 6$ mm, $6 \leqslant d < 8$ mm, $8 \leqslant d < 10$ mm, $10 \leqslant d < 12$ mm, $12 \leqslant d < 14$ mm, $14 \leqslant d < 16$, and $16 \leqslant d < 18$ mm corresponding to mean particle diameter (d_m, (m)) values of 3, 5, 7, 9, 11, 13, 15, and 17 mm, respectively. Additional fractions with $R = 4$ mm ($d_m = 4$, 6, 8, 10, 12, 14, 16 mm), $R = 6$ mm ($d_m = 5$, 7, 9, 11, 13, 15 mm), $R = 8$ mm ($d_m = 6$, 8, 10, 12, 14 mm), $R = 10$ mm ($d_m = 7$, 9, 11, 13 mm), $R = 12$ mm ($d_m = 8$, 10, 12 mm), $R = 14$ mm ($d_m = 9$, 11 mm), and $R = 16$ mm ($d_m = 10$ - mm) and uniform particle size distributions were produced by combining appropriate quantities of the original $R = 2$ mm particle size fractions yielding a total of 36 particle size fractions. Uniform particle size distributions were chosen for two reasons: (I) that biofilter materials are usually available in pre-sorted fractions and (II) to have well-defined and identical particle size distribution shapes for all fractions.

3.2. Filter material characterization

The gravimetric water content of air dry Leca® (determined by drying at 105 °C, for >24 h, until constant weight) was found <1% for all fractions. As this water content is assumed insignificant, air dry Leca® were used without prior drying throughout this study and will be denoted simply as "dry Leca®". Mean dry bulk density (ρ_b (kg m^{-3})) for each particle size fraction was determined in triplicate by filing a 20 L bucket to the edge with dry Leca®, dropping it 3 times from a height of 3–5 cm to achieve a stable packing, and subsequently adding additional material to fill the empty volume created during packing. The Leca® was then weighed. As Leca® is non-expanding when wetted ρ_b is constant regardless of water content (θ, ($m^3\ m^{-3}$)). Based on dry bulk density and a material density of 2.65 g cm^{-3} the total porosity of the media were found to vary between 0.87 and 0.92 $m^3\ m^{-3}$. For each of the fractions with $R = 2$ mm, 10 individual particles were randomly selected and weighed. In addition the diameter of each particle was measured in 3 perpendicular locations (d_1, d_2 and d_3) starting with the widest part of the particle. These data were then used to estimate the specific surface area (a) and the mean particle density (ρ_p, (kg m^{-3})) assuming an ellipsoid particle shape as:

$$\rho_p = \frac{\sum_1^{10}\left(\frac{1}{6}\pi d_{1,i} d_{2,i} d_{3,i}\right)}{M_{tot}} \quad (12)$$

$$a = \rho_b \frac{\sum_1^{10}\left(\frac{\left(4\pi\left(d_{1,i}^{1.6} d_{2,i}^{1.6}\right) + \left(d_{1,i}^{1.6} d_{3,i}^{1.6}\right) + \left(d_{2,i}^{1.6} d_{3,i}^{1.6}\right)\right)}{3}\right)^{1/1.6}}{M_{tot}} \quad (13)$$

where $d_{1,i}$, $d_{2,i}$, $d_{3,i}$ are diameters 1, 2 and 3 of the ith particle and M_{tot} is the total mass of all 10 particles.

The external porosity ε_{ex} for the $R = 2$ mm fractions was then determined as

$$\varepsilon_{ex} = 1 - (\rho_b \rho_p^{-1}) \quad (14)$$

For fractions with R larger than 2 mm ρ_p was calculated as a weighted mean of the particle densities for all 2 mm fractions used in the preparation of these fractions. An overview of a and ε_{ex} for the 36 Leca® particle size fractions is given in Table 1.

Two sets of mass transfer measurements were carried out. The first set involved measurements of transient breakthrough curves in Leca® of selected sparingly soluble organic compounds: Butene, Toluene, Methanethiol (MT), Dimethyl sulfide (DMS), Dimethyl disulfide (DMDS) and Dimethyl trisulfide (DMTS). The second set involved measurement of steady state breakthrough concentrations in Leca® using CO_2 as tracer gas. As it is considerably more difficult and time-consuming to obtain accurate measurements of

Table 1
External volumetric air content (ε_{ex}) and specific surface area (a) of the 36 Leca® fractions with uniform particle size distribution applied in this study. Circles indicate Leca® fractions used in the CO_2 breakthrough experiments and dots indicate Leca® fractions used in the transient breakthrough measurements (Butene, Toluene, MT, DMS, DMDS and, DMTS), and numbers in brackets indicate one standard deviation.

Fraction	ε_{ex} ($m^3\ m^{-3}$)		a ($m^2\ m^{-3}$)	
2–4 mm○●	0.28	(0.005)	1084	(7.4)
4–6 mm○●	0.39	(0.009)	656	(10.2)
6–8 mm○	0.37	(0.003)	508	(2.4)
8–10 mm○●	0.37	(0.001)	372	(0.4)
10–12 mm○	0.36	(0.007)	339	(3.9)
12–14 mm○●	0.33	(0.001)	315	(0.7)
14–16 mm○	0.32	(0.003)	274	(1.3)
16–18 mm○●	0.33	(0.005)	223	(1.8)
2–6 mm○	0.33	(0.002)	866	(2.3)
4–8 mm○	0.37	(0.004)	588	(3.6)
6–10 mm○	0.37	(0.003)	435	(2.2)
8–12 mm○●	0.37	(0.001)	349	(0.5)
10–14 mm○	0.35	(0.009)	325	(4.3)
12–16 mm○	0.28	(0.002)	314	(1.0)
14–18 mm○	0.32	(0.007)	250	(2.5)
2–8 mm○	0.34	(0.007)	735	(7.3)
4–10 mm○	0.37	(0.005)	506	(3.9)
6–12 mm○●	0.37	(0.002)	400	(1.4)
8–14 mm○	0.34	(0.002)	348	(0.8)
10–16 mm○	0.34	(0.002)	307	(1.0)
12–18 mm○	0.31	(0.004)	274	(1.4)
2–10 mm○	0.36	(0.005)	621	(4.5)
4–12 mm○	0.37	(0.002)	463	(1.8)
6–14 mm○	0.35	(0.002)	383	(1.2)
8–16 mm○	0.35	(0.004)	320	(2.1)
10–18 mm○	0.34	(0.001)	285	(0.5)
2–12 mm○	0.35	(0.002)	565	(1.9)
4–14 mm○●	0.36	(0.002)	433	(1.6)
6–16 mm○	0.35	(0.003)	356	(1.6)
8–18 mm○	0.36	(0.002)	291	(1.0)
2–14 mm○	0.35	(0.002)	519	(1.4)
4–16 mm○	0.35	(0.003)	404	(2.0)
6–18 mm○	0.35	(0.002)	331	(1.1)
2–16 mm○●	0.34	(0.003)	481	(2.5)
4–18 mm○	0.34	(0.002)	376	(1.4)
2–18 mm○	0.34	(0.005)	440	(3.7)

Table 2
Particle size fractions, contaminant compound and velocities applied for transient breakthrough curves. Corresponding Henry's constants are in ().

Fraction	V_g = 0.1 (m s^{-1})	V_g = 0.2 (m s^{-1})	V_g = 0.3 (m s^{-1})
2–4 mm	DMTS (0.032)	Butene (9.3), Toluene (0.27), DMS (0.071), DMDS (0.043), DMTS (0.032)	DMTS (0.032)
4–6 mm		DMTS (0.032)	
8–10 mm	DMTS (0.032)	Butene (9.3), Toluene (0.27), DMS (0.071), DMDS (0.043), DMTS (0.032)	DMTS (0.032)
12–14 mm		DMTS (0.032)	
16–18 mm	DMTS (0.032)	Butene (9.3), Toluene (0.27), MT (0.1), DMS (0.071), DMDS (0.043), DMTS (0.032)	DMTS (0.032)
6–12 mm		DMTS (0.032)	
4–14 mm		DMTS (0.032)	
2–16 mm	DMTS (0.032)	Butene (9.3), Toluene (0.27), DMS (0.071), DMDS (0.043) DMTS (0.032)	DMTS (0.032)

transient break-through curves for sparingly soluble, odorous, organic compounds, the first set of measurements were carried out for selected Leca® fractions. The CO_2 breakthrough measurements were carried out for all Leca® fractions as these measurements are considerably simpler and faster to perform. An overview of the Leca® fractions used in the two sets of measurements is given in Table 1.

3.3. Transient condition odorous compound breakthrough measurements

Measurements of transient breakthrough curves were performed using a filter unit connected to a CUBUFAN 160 EC ventilation pump (Jenk, Brøndby, Denmark) supplying a downward airflow through the filter medium. Air flow through the Leca® was measured continuously in the inlet to the pump using a VA400 thermal mass flow sensor, (CS instruments Tannheim Germany). The general airflow velocity varied from 0.1 to 0.3 m s^{-1} giving empty bed retention times (EBRT) of 3–11 s which corresponds well to previously published biofilter studies [7,13,30,31]. Each fraction of Leca® was wetted to its maximum water holding capacity via immersion in water for a period of at least 3 days (no significant weight gain was observed for periods exceeding 3 days) followed by drainage for 2 h. After drainage each fraction was packed into a vertical Ø25 cm steel ventilation tube to a height of approximately 100 cm. As the same filter material was repacked at every measurement, small variation in height was observed (up to 2 cm). This variation and the corresponding porosity change were included in the model. A nozzle spraying deionized water at a rate of 1 L h^{-1} (0.02 m h^{-1}) was mounted 36 cm above the Leca® filter inlet. The nozzle was fed with a mixture of water and pressurized air in order to achieve adequate water distribution across the inlet surface of the filter. Sampling tubes were mounted 23 cm above the filter inlet and 14 cm below the filter outlet, respectively. Through each of these tubes air was sampled continuously at a flow rate of 100 L h^{-1}. The air was led to a commercial high-sensitivity Proton-Transfer-Reaction Mass Spectrometry (PTR-MS) (Ionicon Analytik, Innsbruck, Austria) where odorous compound concentration in the sample air was measured with a frequency of 0.152 s^{-1}. The odorous compounds were injected directly into the airstream at a point 2.6 m before the filter inlet to ensure adequate distribution of the compound in the air stream at the filter inlet. Injection of each odorous compound was done from a pressurized gas cylinder via a flow controller and a magnetic valve controlled by the PTR-MS, to a maximum outlet concentration of (1.5×10^{-4}–1.5×10^{-2} g m^{-3}, dependent gas velocity and compound characteristics). Measurements for each compound were carried out separately as the PTR-MS can only detect one compound at a time. A schematic of the experimental setup is given in Fig. 1. A more detailed description of the experimental setup can be found in [32]. Each compound injection was carried out as a pulse lasting 20 s, followed by a continuous "clean" airstream for about 150 s. Due to the very short filter retention time (1–3 s) it was not possible to conduct concentration measurements in multiple locations (inlet and outlet) simultaneously with sufficient accuracy. Thus, it was not possible to measure the breakthrough curves belonging to the same injection event at both the filter inlet and outlet. To compensate for this, five consecutive inlet curves, followed by five outlet curves and finally followed by three consecutive inlet curves (corresponding to 13 consecutive injection events) were measured for each compound. The final three inlet curves were measured to verify the stability of the injected mass flow during the course of each experiment. Measurements of transient breakthrough curves were carried out using six different organic odorous compounds at three different V_g for eight different Leca® particle size fractions, yielding a total of 429 individual breakthrough curves. An overview of the compounds, particle size fractions, and air flow velocities used in the transient experiments, is given in Table 2, A more detailed description of the method can be found in Ref. [32].

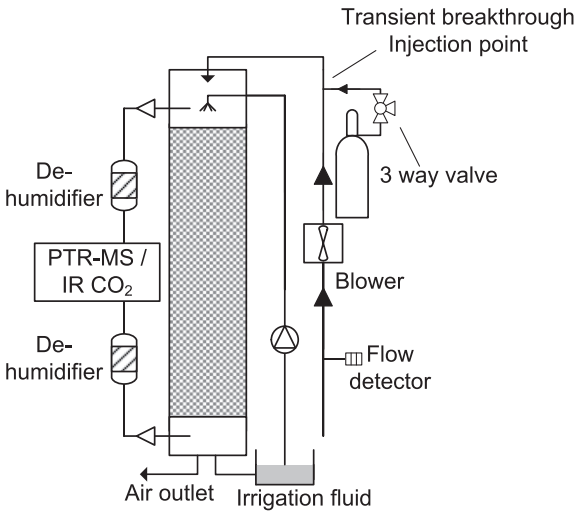

Fig. 1. Experimental setup for steady state and transient breakthrough measurements. Injections were only applied for the transient breakthrough measurements.

3.4. Steady state condition CO_2 breakthrough measurements

Steady state CO_2 breakthrough concentrations were measured for all 36 Leca® fractions including the 8 fractions used in the transient breakthrough measurements. Prior to the first experiment each Leca® fraction was immersed in 1 M NaOH solution for 1 h, followed by drainage for 10 min. For replicate measurements a 10 min immersion and 10 min drainage period was used. After drainage each fraction was packed into a vertical Ø23.5 cm PVC tube to a height of 30 cm. A nozzle spraying 1 M NaOH at a rate of 1 L h^{-1} (0.02 m h^{-1}) was mounted 42 cm above the filter inlet. Sampling tubes for monitoring in and outlet CO_2 concentrations were mounted 2 cm above the filter inlet and 8 cm below the filter outlet, respectively. The NaOH soaked media was fed with ambient air (inlet CO_2 measured to ≈0.6–0.7 g m^{-3}) at V_g = 0.2 m s^{-1}. Steady state was achieved 1 min after the airflow was initiated and consecutive in and outlet CO_2 measurements were done by extracting a flow of 3 L h^{-1} via the in- and outlet sampling tubes and directing these to a glass vial containing an EXTECH, SD800 NDIR (non-dispersive infrared) CO_2 detector. The duration of both in and outlet

measurements were around 2 min adding up to 5 min of airflow for each complete $k_g a_e$ determination. The pH of the NaOH solution being sprayed on the filter material was monitored throughout the experiment using MERCK pH strips in order to ensure pH > 14. All measurements were carried out in duplicates.

3.5. Mass transfer modeling

Average in and outlet breakthrough curves for each combination of odorous compound, Leca® particle size fraction and air velocity were calculated by averaging the individual measured in and outlet breakthrough curves for each combination. Eqs. (4a) and (4b) were solved numerically in Exel using an explicit finite difference model. This model was then fitted to the measured transient breakthrough data. Breakthrough curves of Butene (which has an extremely low solubility in water) showed that dispersion was negligible (setting the dispersion coefficient to 0 showed insignificant impact on model predictions) and dispersion was therefore omitted from the data fitting. Because θ_a could not be estimated independently, the model was fitted to the measured data using θ_a and $K_G a_e$ as fitting parameters. This yielded θ_a values of 30% of the total water content on average.

Mass transfer generally has a stronger influence on the tail profile of the outlet breakthrough curves compared to the initial (increasing) part. To obtain the most accurate estimate, the optimal values of $K_G a_e$ and θ_a were therefore determined by fitting the model to the breakthrough data in the period from the observed maximum concentration to the point where the measured outlet was less than 1% of the maximum concentration. As the residence time for the liquid phase on average was 140 times higher than for the gas phase the liquid phase was assumed immobile in the model calculations. Sorption was likewise ignored for the following reasons: Full mass recovery was observed in all experiments indicating no irreversible sorption. Calculations based on measured data for methanethiol sorption onto dry Leca [33] indicated that <0.01% of the total mass applied during our experiments would sorb under dry conditions. Under moist conditions sorption would be even less. As sorption behavior for the other odorous compounds used in this study is similar to methanethiol negligible sorption was also assumed for them.

Average values of the effluent steady state CO_2 concentration for each Leca® particle size fraction were initially calculated. Corresponding values of $K_G a_e$ for the steady state CO_2 mass transfer were then determined using Eq. (5).

4. Results

4.1. Filter media characteristics

Although d_m and R varied with more than 450% and 700%, respectively, across the 36 filter media only a 40% variation was observed for ε_{ex} while a varied with 390%. The Leca® materials therefore represent a very large range of particle diameters and specific surface areas.

4.2. Relating mass transfer and gas velocity

Odorous compound outlet breakthrough curves generally exhibited retardation and increased tailing compared to the inlet curves for all filter materials investigated. This is illustrated in Fig. 2, where in- and outlet curves for DMTS in the 2–4 and 16–18 mm Leca® fractions are shown, indicating non-equilibrium air–water phase mass transfer of the odorous compounds.

The model (Eqs. (4a) and (4b)) was found to fit the tailing profile of the measured outlet concentration data very well (Fig. 2) with a root mean square error (RMSE), on average, observed to constitute less than 1% of the observed maximum concentration in the outlet. The model also matches the initial (increasing) part of the measured breakthrough curves relatively well (Fig. 2) despite not being fitted to these data.

To evaluate the relationship between $K_G a_e$ and u, Eq. (11) was fitted to $K_G a_e$–u data for the Leca® particle size fractions where more than one u-value was used (12 combinations of velocity and particle size fraction measured for DMTS). It was observed that although a depended on d_m and R, for each particle size fraction β was independent of the particle fraction used. Fitted $K_G a_e \alpha^{-1}$ vs. u data are shown in Fig. 3 and resulting values of α and β as well as model RMSE are given in Table 3.

$K_G a_e$ increases with u for all particle fractions investigated (Fig. 3). Increasing $K_G a_e$ as a function of u have also been reported by [8,12,24,26], and the value of $\beta = 0.82$ is very close to the value of 0.7 proposed by Onda et al. [8] for $k_g a_e^{-1} \gg H\, k_l a_e^{-1}$, at as well as the range of 0.02–0.75 suggested by Kim and Deshusses [12] at similar conditions. The parameter α is seen to decrease with increasing d_m and R (note for R only two measurements are available) which is likely because a_e is inversely proportional to these parameters.

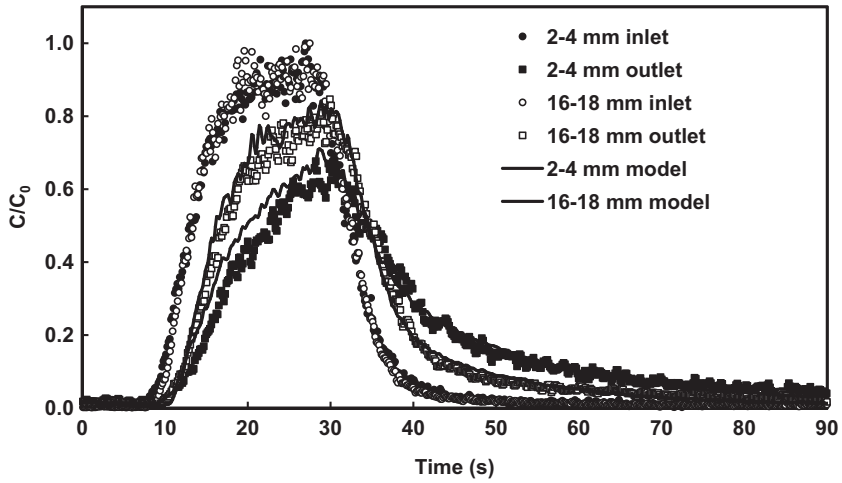

Fig. 2. Measured relative in- and outlet curves of DMTS in 2–4 and 16–18 mm Leca®. C_0 is taken as the maximum observed inlet concentration.

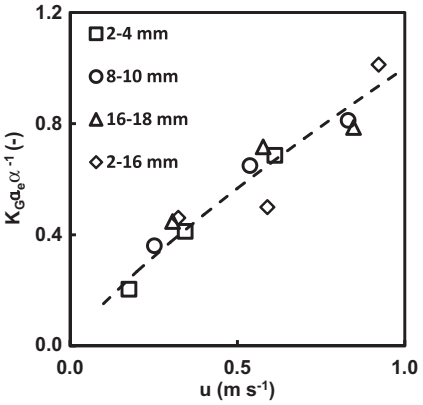

Fig. 3. $K_G a_e \alpha^{-1}$ (DMTS) vs. pore gas velocity (u). Solid line is Eq. (11) with $\beta = 0.82$.

Table 3
Empirical model parameters for Eq. (11) and corresponding RMSE.

k (s^{-1})	P	α	β	RMSE (s^{-1})
$K_G a_e$	u (m s^{-1})	$\alpha_{2-4mm} = 0.66$, $\alpha_{8-10mm} = 0.44$, $\alpha_{16-18mm} = 0.24$ and $\alpha_{2-16mm} = 0.37$	0.82	0.03
$K_G a_e$	H (–)	$\alpha_{2-4mm} = 0.0.0137$, $\alpha_{8-10mm} = 0.0090$, $\alpha_{16-18mm} = 0.0052$ and $\alpha_{2-16mm} = 0.0069$	−1	0.03
$K_G a_e$	α (m^2 m^{-3})	0.015	0.49	0.02
$k_g a_e$	α (m^2 m^{-3})	0.0017	1.18	0.42
$K_G a_e$	$k_g a_e$ (s^{-1})	0.24	0.33	0.03
$K_G a_e$	d_{eq} (m)	0.040	−0.41	0.03
$k_g a_e$	d_{eq} (m)	0.028	−0.85	0.53
$K_G a_e$	$d_{eq}\alpha^{-1}$ (m^2)	0.025	−0.22	0.02
$k_g a_e$	$d_{eq}\alpha^{-1}$ (m^2)	0.0057	−0.53	0.40

4.3. Relating H and mass transfer

Fig. 5a shows $K_G a_e$ for Butene, Toluene, MT, DMS, DMDS and DMTS as a function of H for the 2–4, 8–10, 16–18, and 2–16 mm Leca® particle size fractions at $V_g = 0.2$ m s^{-1}. In all cases $K_G a_e$ decreases with increasing H in a hyperbolic manner. This suggests that for constant u it is the second term on the right-hand side of Eq. (6) that is most important and $K_G a_e$ can therefore be expressed by Eq. (11) with $k = K_G a_e$, $\alpha = k_l a_e$, P = H, and $\beta = -1$. This means that a plot of $K_G a_e\, k_l a_e^{-1} = K_G k_l^{-1}$ vs. H^{-1} should yield a straight line with a slope of 1. To verify this Eq. (11) with $k = K_G a_e$, $a = k_l a_e$, P = H, and $\beta = -1$ was fitted to the H–$K_G a_e$, data for Butene, Toluene, MT, DMS, DMDS and DMTS using $\alpha = k_l a_e$ as fitting parameter, fitted individually for each particle size fraction, yielding a total of 4 fitting parameters to model the 21 $K_G a_e$ measurements. Fig. 5b shows the resulting values for $K_G k_l^{-1}$ as a function of H^{-1} while values of the fitting parameter $k_l a_e^{-1}$ are given in Table 3. The relationship between $K_G k_l^{-1}$ and H^{-1} yields a straight line with a slope of 1.002 and a R^2 of 0.93 indicating that the assumption that $K_G a_e$ are inversely related to H is valid at least within the range of particle sizes and H's considered here. The fitted values of $k_l a_e^{-1}$ decreases with increasing particle size as would be expected (Table 3). The data in Fig. 3 (indicating that the gas phase mass transfer term $k_g a_e$ in Eq. (6) is limiting) and the data in Fig. 4 (indicating that the liquid phase mass transfer is limiting) appear contradictory at a first glance. The explanation is probably that it is the liquid side mass transfer that is limiting (as the compounds used are only sparingly soluble) but that the liquid phase mass transfer is influenced by the gas phase flow velocity (in contrast to Onda et al. [8]). Several studies have found experimental evidence for a_e to increase with increasing u even if the liquid phase mass transfer is limiting. This is because the gas flow cause instabilities in the air water interphase such as ripples, waves and creation of droplets [28,34] and further reduces the amount of stagnant air zones unavailable for mass transfer [35]. Thus $K_G a_e$ can be proportional to u even in situations when in $K_G a_e$ is not restricted by the gas side mass transfer according to the two-film theory ($H\, k_l a_e^{-1} \gg k_g a_e^{-1}$).

4.4. Relating mass transfer and media specific surface area

Fig. 6 shows $K_G a_e$ for DMTS vs. a for the eight particle size fractions in Table 1. In addition CO_2 mass transfer data (measured for all 36 particle size fractions with the liquid side mass transfer resistance eliminated, thus $K_G a_e = k_g a_e$) are shown. Both the observed $K_G a_e$ (DMTS) and $k_g a_e$ (CO_2) increase with increasing a in agreement with Onda et al. [8] (Eqs. (7) and (8)). The $K_G a_e$–a data seem to follow the same relationship (with the exception of the 2–16 mm fraction which is regarded as an outlier and therefore omitted in the subsequent data fitting) regardless of the particle size fraction (values of d_m and R) considered. The same is also the case for the $k_g a_e$–a data although the $k_g a_e$ values on average are about 9 times higher than the corresponding $K_G a_e$ values. This confirms that the liquid side mass transfer term in Eq. (6) ($H\, k_l a_e^{-1}$) is limiting $K_G a_e$ as also discussed above. The relationships between $K_G a_e$ and a for the odorous compound and for the CO_2 mass transfer data were fitted by Eq. (11) with $k = K_G a_e$, and P = a, using α and β as fitting parameters that were chosen to be independent of the particle size and thus valid for all particle size fractions used. In this

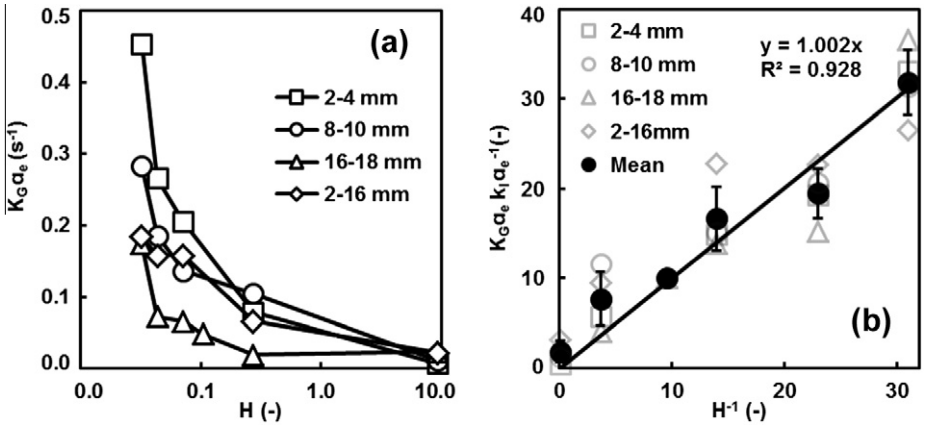

Fig. 4. (a) Observed $K_G a_e$ vs. Henry's constant (H) measured for six different compounds: Butene, Toluene, MT, DMS, DMDS and DMTS in 4 different particle size distributions. (b) Observed $K_G a_e$ (fitted $k_l a_e)^{-1}$ vs. H^{-1} Gray marked, white filled symbols are measurements and black filled circles are mean values. Bars represent standard deviations.

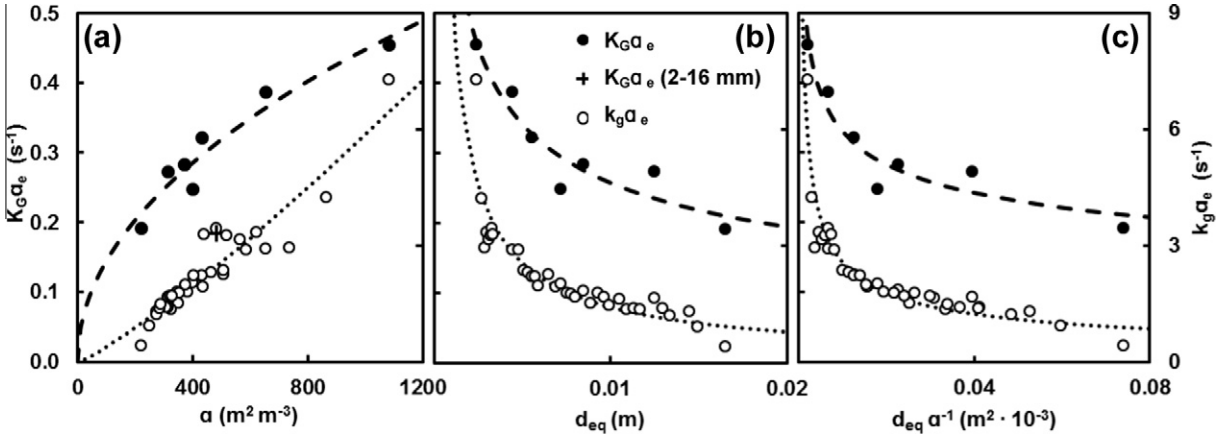

Fig. 5. $K_G a_e$ for DMTS and $k_g a_e$ found by CO_2 reaction method vs.: (a) media specific surface area (a), dashed line represent Eq. (11) ($\alpha = 0.015$, $\beta = 0.49$) and dotted line represent Eq. (11) ($\alpha = 0.0017$, $\beta = 1.18$). (b) d_{eq}, dashed line represent Eq. (11) ($\alpha = 0.040$, $\beta = -0.41$) and dotted line represent Eq. (11) ($\alpha = 0.028$, $\beta = -0.85$). (c) d_{eq}/a dashed line represent Eq. (11) ($\alpha = 0.025$, $\beta = -0.22$) and dotted line represent Eq. (11) ($\alpha = 0.0057$, $\beta = -0.53$).

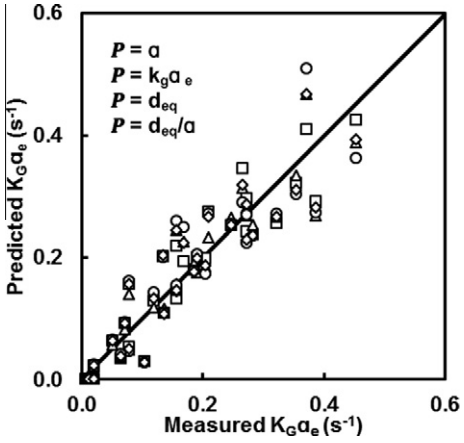

Fig. 6. Measured and predicted values of $K_G a_e$ based on Eq. (16) with $P = a$, $P = k_g a_e$, $P = d_{eq}$ or $P = d_{eq}/a$.

case the parameter α corresponds to $(k_g^{-1} + H\, k_l^{-1})^{-1}$ and β accounts for the deviations between a and a_e. An overview of the resulting values is given in Table 3. The value of $\beta = 0.49$ for the odorous compounds is within the range (0.33–1.3) proposed by Onda et al. [8] (Eqs. (7) and (8)) based on the two film theory (Eq. (6)) assuming that $(a_e a^{-1})$ is constant. The value of $\beta = 1.18$ for CO_2 is corresponding to Onda et al. [8] who found $k_g a_e$ proportional to $a^{1.3}$ for media consisting of uniformly sized spherical particles (Eq. (7), note that for uniform spherical particles $a = 6(1 - \varepsilon_{ex})\, d_m^{-1}$)) meaning increasing k_g for decreasing particle size. A value of $\beta > 1$ could also be caused by an increased $a_e a^{-1}$ ratio at decreasing particle size but as $\beta < 1$ for $K_G a_e$ vs. a this explanation seems implausible. Furthermore $\beta = 0.49$ for $K_G a_e$ and 1.18 for $k_g a_e$ β indicate that k_l is related to surface area in a different manner than k_g as found by Onda et al. [8] (Eqs. (7) and (8)). The results of fitting the $K_G a_e$–a and the $k_g a_e$–a relationships (Table 3, Fig. 5a) indicate that once the relationship between $K_G a_e$ and $k_g a_e$ have been established for a given type of material (in this study Leca®) based on a limited set of measurements, further estimates of $K_G a_e$ for specific particle size fractions can be based on $k_g a_e$ measurements. As $k_g a_e$ are not limiting $K_G a_e$ this correlation between $K_G a_e$ and $k_g a_e$ are facilitated by their common dependency of a (Fig. 5a, Eqs. (6)–(8)), rather than a true $K_G a_e$–$k_g a_e$ dependency. Eq. (11) with $k = K_G a_e$, and $P = k_g a_e$, using α and β as fitting parameters, valid for all particle size fractions used, were found to fit the observed $K_G a_e$ data well (Table 3) thus $k_g a_e$ for this material can be used to estimate $K_G a_e$. As the measurements of $k_g a_e$ are much simpler, steady state measurements these can be performed in large numbers at low cost compared to the much more time consuming and expensive $K_G a_e$ measurements requiring access to expensive equipment such as a PTR-MS and the use of numerical data fitting.

When designing cost effective granular biofilter media of different sized particles, knowledge of media $K_G a_e$ as a function of particle size distribution is preferable as it is normally the particle size distribution that is known rather than the specific surface area. As specific surface area and particle size distribution are related it should be possible to relate $K_G a_e$ to a representative particle diameter for a given particle size fraction from a specific material using the same approach as used above for a. Andreasen and Poulsen [1] proposed for Leca® particle size fractions an equivalent particle diameter d_{eq} expressed as:

$$d_{eq} = \frac{2}{\frac{1}{d_m} + \frac{1}{d_{m-\frac{R}{2}}}} \tag{15}$$

The d_{eq}–$K_G a_e$ and d_{eq}–$k_g a_e$ relationships are shown together with fitted Eq. (11) with $P = d_{eq}$ in Fig. 5b. Resulting values of α and β are shown in Table 3. Fig. 5b shows that it is possible to get a close fit of both relationships indicating that the approach for predicting $K_G a_e$ and $k_g a_e$ based on d_{eq} is valid. The RMSE for Eq. (11) is slightly higher for $P = d_{eq}$ compared to Eq. (11) with $P = a$, however $k_g a_e$ based on Eq. (11) with $P = d_{eq}$ vs. $P = a$ was found to exhibit less scatter. This decline in scatter could be explained by the fact that d_{eq} is more closely linked to the media flow characteristics [1] and thereby to the shape and size of the media pores. To test if $P = d_{eq} a^{-1}$ would improve the performance of Eq. (11), Eq. (11) with $P = d_{eq} a^{-1}$, and $k = K_G a_e$ or $k_g a_e$ were fitted to the data using α and β as fitting parameters (Fig. 5c and Table 3). Eq. (11) with $P = d_{eq} a^{-1}$ was observed to have similar RMSE as with $P = a$, for both $K_G a_e$ and $k_g a_e$ prediction but with a reduced scatter of the $k_g a_e$ data.

4.5. Predicting $K_G a_e$ in granular biofilter media

The relationships for predicting $K_G a_e$ for sparingly soluble odorous compounds in biofilter media identified in this study (Table 3) suggest that $K_G a_e$ may be predicted from corresponding values of u and H in combination with either a, $k_g a_e$ (for instance measured using CO_2), d_{eq} or $d_{eq} a^{-1}$. Based on the relationships between $K_G a_e$ and the individual parameters u, H, a, d_{eq} and $d_{eq} a^{-1}$ as discussed above it was chosen to model $K_G a_e$ as:

$$K_G a_e = \alpha u^{\beta_u} H^{-1} P^{\beta_p} \tag{16}$$

Table 4
Calibrated constants and cross validated RMSE Eq. (16).

P	Calibrated constants			RMSE
	α	β_v	β_p	Validation (s^{-1})
α ($m^2\ m^{-3}$)	75×10^{-5}	0.70	0.47	0.04
$k_g a_e$ (s^{-1})	0.010	0.65	0.28	0.04
d_{eq} (m)	0.003	0.60	−0.31	0.05
$d_{eq}a^{-1}$ (m^2)	0.001	0.65	−0.20	0.05

where α, β_u and β_p are empirical constants, valid across all particle size fractions, and P is either a, $k_g a_e$, d_{eq} or $d_{eq}a^{-1}$. Eq. (16) was cross validated against all $K_G a_e$ data shown in Figs. 3–5, a total of 33 $K_G a_e$ values obtained for three different u, six different H and seven different combinations of d_m and R. The cross validation was carried out as follows: Eq. (16) was calibrated to 32 out of the 33 $K_G a_e$ measurements using α, β_u, and β_p as calibration (fitting) parameters. Eq. (16) with the calibrated values of α, β_u, and β_p, was then used to predict the $K_G a_e$ value not used in the fitting. The calibration–validation approach was repeated 33 times each time using a different $K_G a_e$ measurement for the validation yielding a total of 33 predictions, all of which based on constants calibrated on different data than applied for its validation. This procedure was repeated for $P = a$, $P = k_g a_e$ $P = d_{eq}$ and $P = d_{eq}a^{-1}$. Measured and predicted values of $K_G a_e$ using Eq. (16) with $P = a$, $P = k_g a_e$, $P = d_{eq}$ or $P = d_{eq}/a$ are shown in Fig. 6 and the corresponding values of α, β_u, and β_p (based on all data) as well the cross validated RMSE are shown in Table 4. Using $P = a$, $P = k_g a_e = d_{eq}$ or $P = d_{eq}/a$ yielded similar prediction accuracy (Table 4). This means that $K_G a_e$ may be predicted using u and H in combination with either a, $k_g a_e$, d_{eq} or $d_{eq}a^{-1}$ based on convenience. In cases where biofilter materials have a known uniform particle size distribution (which is the case for many artificial materials), predictions based on u and H in combination with d_{eq} may be most convenient. Alternatively if the particle size distribution is unknown estimates of $K_G a_e$ may be made based on u and H in combination with $k_g a_e$ measured using for instance CO_2 absorption.

As the models presented in this paper have been developed based on mass transfer data for Leca® with particle diameters of 2–18 mm and a rounded shape, the developed models are theoretically only valid for media produced from this material. However, as mass transfer and fluid flow in porous media follow the same basic principles regardless of medium properties, it is likely that the model concept presented here is applicable to a much wider range of particle sizes and material types than considered here. As fluid flow in porous materials also depends on particle shape [36], this means that the empirical constants in Table 4 are likely also dependent on particle shape. It is further noted that the results presented in this paper were based on materials where no microbial biomass was present. Presence of a biofilm will very likely alter a_e as biomass is known to affect media airflow characteristics [37] and has been observed to increase solubility of hydrophobic compounds [18] thereby increasing H and the corresponding $K_G a_e$.

Filter media cost efficiency is often measured as the filter efficiency, divided by the cost. Assuming efficiency to be proportional to packing media $K_G a_e$, and operation costs to be proportional to the energy consumption and thereby the specific pressure drop across the filter, filter operational cost efficiency is proportional to $K_G a_e/(\Delta P/L)$, where ΔP is pressure drop and L is filter length in the direction of flow.

To illustrate the use of the $K_G a_e$–d_{eq} relationship established in this paper to select the optimal biofilter medium particle size distribution taking into account filter energy consumption (due to filter pressure drop) a $\Delta P/L$–d_{eq} relationship for the media utilized in this study [1] was used:

$$\frac{\Delta P}{L} = 142\left(d_{eq}\left(1+\frac{5.28\times10^{-9}\ \mathrm{m}^3}{\left(d_m-\frac{R}{2}\right)^3}\right)\right)^{-2}\mu V + 10.82\left(d_{eq}\left(1+\frac{5.28\times10^{-9}\ \mathrm{m}^3}{\left(d_m-\frac{R}{2}\right)^3}\right)\right)^{-1}\rho V^2 \quad (17)$$

Combining Eqs. (16) and (17) with $P = d_{eq}$, and simplifying, the proportionality between $K_G a_e/(\Delta P/L)$ vs. d_m and R can be expressed as:

$$\frac{K_G a_e}{\Delta P/L} \propto \left(1+\frac{5.28\times10^{-9}\ \mathrm{m}^3}{\left(d_m-\frac{R}{2}\right)^3}\right)^2 d_{eq}^{1.69} \quad (18a)$$

at low Re (high V, viscous forces dominating $\Delta P/L$)

$$\frac{K_G a_e}{\Delta P/L} \propto \left(1+\frac{5.28\times10^{-9}\ \mathrm{m}^3}{\left(d_m-\frac{R}{2}\right)^3}\right) d_{eq}^{0.69} \quad (18b)$$

at high Re (high V, inertial forces dominating $\Delta P/L$).

Within the applicable range of Eqs. (16) and (17) (d_m = 3–17 mm, R = 2–16) Eqs. (18a) and (18b) state the highest $K_G a_e/(\Delta P/L)$ value to be obtained at maximum d_m (17 mm) and minimum R (2 mm). It should be noticed that construction cost are not included, and that the inclusion of such will benefit a reduced particle size as the use of smaller particles requires smaller filters. It should further be noticed that accumulation of biomass within the biofilter media are known to increase biofilter $\Delta P/L$ in a hyperbolic manner, until complete filter clogging [37]. As smaller pores seems more sensitive for clogging than larger pores this argument further favors the application of large particles.

5. Conclusions

In this study the relationships between the overall air–water phase mass transfer coefficients ($K_G a_e$) for sparingly soluble organic compounds in coarse granular porous material and material physical properties were investigated using Leca® (Lightweight Expanded Clay aggregates). As $K_G a_e$ of sparingly soluble organic compounds cannot be measured directly (as without chemical removal of the compounds in the water phase) using the traditional steady state mass transfer procedures, $K_G a_e$ was measured based on transient breakthrough curves.

Measurements of $K_G a_e$ were carried out using six different organic odorous compounds at three different gas velocities for eight different Leca® particle size fractions constituting a total of 429 individual breakthrough curves. Additional steady state mass transfer experiments using CO_2 were carried outfor 36 different Leca® particle size fractions. $K_G a_e$ was found to be proportional to the specific surface area (a), the equivalent particle diameter (d_{eq}), and ($d_{eq}a^{-1}$). In addition $K_G a_e$ depended on both the pore gas velocity (u) and Henrys constant for the individual organic compounds (H). A set of power function expressions relating $K_G a_e$ to u, H, and either a, d_{eq}, or $d_{eq}a^{-1}$ or measured CO_2 mass transfer data, were developed based on 3 empirical constants (α, β_V and β_P) and successfully validated (RMSE $\leqslant$ 25% of average $K_G a_e$) across u, H and a varying by up to 500%, 29,000% and 500% respectively.

In essence this means that α, β_V and β_P for a specific particle size fraction originating from a given material (for instance Leca®) can be established based on a limited set of transient $K_G a_e$ measurements, in combination with knowledge of a, d_{eq}, $d_{eq}a^{-1}$ or measured steady state mass transfer data (using for instance CO_2). Hereafter $K_G a_e$ for any other particle size fraction for that same material as a function of, u and H can be predicted. As measurement of $K_G a_e$ based on transient breakthrough curves is quite time-consuming, significant time savings may be achieved using the approaches presented here if knowledge of $K_G a_e$ for different particle size fractions originating from the same material is

needed. Such knowledge is valuable when selecting optimal particle size distribution for granular biofilter media.

Acknowledgements

The authors wish to thank Knud Mortensen (Saint-Gobain Weber A/S) and his Leca® sorting crew for providing the well sorted Leca® fractions used in the experiments.

References

[1] R.R. Andreasen, T.G. Poulsen, Air flow characteristics in granular biofilter media, J. Environ. Eng., (2013). <http:dx.doi.org/10.1061/(ASCE)EE.1943-7870.0000640> [E-Pub ahead of print].
[2] P. Best, World pork output grows again, in: Pig international, <WATTAgNet.com>, 2010, pp. 8–9.
[3] S.S. Schiffman, E.A. Sattely Miller, M.S. Suggs, B.G. Graham, The effect of environmental odors emanating from commercial swine operations on the mood of nearby residents, Brain Res. Bull. 37 (1995) 369–375.
[4] D.H. O'Neill, I.W. Stewart, V.R. Phillips, A review of the control of odour nuisance from livestock buildings: Part 2, the costs of odour abatement systems as predicted from ventilation requirements, J. Agric. Eng. Res. 51 (1992) 157–165.
[5] L. Chen, S.J. Hoff, Mitigating odors from agricultural facilities: a review of literature concerning biofilters, Appl. Eng. Agric. 25 (2009) 751–766.
[6] N.J.R. Kraakman, J. Rocha-Rios, M.C.M. van Loosdrecht, Review of mass transfer aspects for biological gas treatment, Appl. Microbiol. Biotechnol. 91 (2011) 873–886.
[7] A. Feilberg, A.P.S. Adamsen, S. Lindholst, M. Lyngbye, A. Schafer, Evaluation of biological air filters for livestock ventilation air by membrane inlet mass spectrometry, J. Environ. Qual. 39 (2010) 1085–1096.
[8] K. Onda, H. Takeuchi, Y. Okumoto, Mass transfer coefficients between gas and liquid phases in packed columns, J. Chem. Eng. Jpn. 1 (1968) 56.
[9] M.C. Delhomenie, L. Bibeau, M. Heitz, A study of the impact of particle size and adsorption phenomena in a compost-based biological filter, Chem. Eng. Sci. 57 (2002) 4999–5010.
[10] I.M. Scotford, C.H. Burton, V.R. Phillips, Minimum-cost biofilters for reducing odours and other aerial emissions from livestock buildings. 2. A model to analyse the influence of design parameters on annual costs, J. Agric. Eng. Res. 64 (1996) 155–163.
[11] G. Leson, A.M. Winer, Biofiltration – an innovative air-pollution control technology for voc emissions, J. Air Waste Manag. Assoc. 41 (1991) 1045–1054.
[12] S. Kim, M.A. Deshusses, Determination of mass transfer coefficients for packing materials used in biofilters and biotrickling filters for air pollution control – 2: development of mass transfer coefficients correlations, Chem. Eng. Sci. 63 (2008) 856–861.
[13] A.D. Dorado, G. Rodriguez, G. Ribera, A. Bonsfills, D. Gabriel, J. Lafuente, X. Gamisans, Evaluation of mass transfer coefficients in biotrickling filters: experimental determination and comparison to correlations, Chem. Eng. Technol. 32 (2009) 1941–1950.
[14] B. Deheyder, A. Overmeire, H. Vanlangenhove, W. Verstraete, Ethene removal from a synthetic waste-gas using a dry biobed, Biotechnol. Bioeng. 44 (1994) 642–648.
[15] A.M. Nielsen, L.P. Nielsen, A. Feilberg, K.V. Christensen, A method for estimating mass-transfer coefficients in a biofilter from membrane inlet mass spectrometer data, J. Air Waste Manag. Assoc. 59 (2009) 155–162.
[16] W.A.S. Saint-Gobain, Leca® letklinker anvendt som filtermateriale, 2011.
[17] L. Nielsen, N. Nørgaard, Annual report 2010, Pig Research Centre, 2010, p. 28.
[18] B.H. Davison, J.W. Barton, K.T. Klasson, A.B. Francisco, Influence of high biomass concentrations on alkane solubilities, Biotechnol. Bioeng. 68 (2000) 279–284.
[19] J.W. Barton, C.D. Vodraska, S.A. Flanary, B.H. Davison, Solubility of toluene, benzene and TCE in high-microbial concentration systems, Chemosphere 73 (2008) 1737–1740.
[20] J.W. Barton, C.D. Vodraska, S.A. Flanary, B.H. Davison, Partitioning of btex constituents and chloroorganics in high-biomass systems, Environ. Prog. 22 (2003) 95–102.
[21] J.D. Istok, Groundwater modeling by the finite element method, Amer Geophysical Union, 1989.
[22] K. Onda, E. Sada, H. Takeuchi, Gas absorbtion with chemical reaction in packed coloumns, J. Chem. Eng. Jpn. 1 (1968) 62–66.
[23] W.K. Lewis, W.G. Whitman, Principles of gas absorption, Ind. Eng. Chem. 16 (1924) 1215–1220.
[24] P.V. Roberts, G.D. Hopkins, C. Munz, A.H. Riojas, Evaluating two-resistance models for air stripping of volatile organic contaminants in a countercurrent, packed column, Environ. Sci. Technol. 19 (1985) 164–173.
[25] G.Q. Wang, X.G. Yuan, K.T. Yu, Review of mass-transfer correlations for packed columns, Ind. Eng. Chem. Res. 44 (2005) 8715–8729.
[26] B.I. Dvorak, D.F. Lawler, J.R. Fair, N.E. Handler, Evaluation of the Onda correlations for mass transfer with large random packings, Environ. Sci. Technol. 30 (1996) 945–953.
[27] J. Staudinger, W.R. Knocke, C.W. Randall, Evaluating the Onda mass-transfer correlation for the design of packed-column air stripping, J. Am. Water Work Assoc. 82 (1990) 73–79.
[28] J.L. Bravo, J.R. Fair, Generalized correlation for mass-transfer in packed distillation-columns, Ind. Eng. Chem. Process Des. Dev. 21 (1982) 162–170.
[29] S. Kim, M.A. Deshusses, Determination of mass transfer coefficients for packing materials used in biofilters and biotrickling filters for air pollution control. 1. Experimental results, Chem. Eng. Sci. 63 (2008) 841–855.
[30] L.D.M. Ottosen, S. Juhler, L.B. Guldberg, A. Feilberg, N.P. Revsbech, L.P. Nielsen, Regulation of ammonia oxidation in biotrickling airfilters with high ammonium load, Chem. Eng. J. 167 (2011) 198–205.
[31] W.J. Swanson, R.C. Loehr, Biofiltration: fundamentals: design and operations principles: and applications, J. Environ. Eng. – ASCE 123 (1997) 538–546.
[32] D. Liu, R.R. Andreasen, T.G. Poulsen, A. Feilberg, Experimental determination of mass transfer coefficients for volatile sulfur odorants in biofilters measured by proton-transfer-reaction mass spectrometry (PTR-MS), Chem. Eng. J. (2013), http://dx.doi.org/10.1016/j.cej.2012.1012.1088 [E-Pub ahead of print].
[33] R.K. Tabase, Chemisorption of Hydrogen Sulphide and Methanethiol by Light Expanded Clay Agreagate (LECA), Department of Biosystems Engineering Århus University, Århus, 2011.
[34] M.H. Debrito, U. Vonstockar, A.M. Bangerter, P. Bomio, M. Laso, Effective mass-transfer area in a pilot-plant column equipped with structured packings and with ceramic rings, Ind. Eng. Chem. Res. 33 (1994) 647–656.
[35] F.X. Prenafeta-Boldu, J. Illa, J.W. van Groenestijn, X. Flotats, Influence of synthetic packing materials on the gas dispersion and biodegradation kinetics in fungal air biofilters, Appl. Microbiol. Biotechnol. 79 (2008) 319–327.
[36] I.F. Macdonald, M.S. Elsayed, K. Mow, F.A.L. Dullien, Flow through porous-media – Ergun equation revisited, Ind. Eng. Chem. Fundam. 18 (1979) 199–208.
[37] R.R. Andreasen, R.E. Nicolai, T.G. Poulsen, Pressure drop in biofilters as related to dust and biomass accumulation, J. Chem. Technol. Biotechnol. 87 (2012) 806–816.